FULL PAPER

Dalton
www.rsc.org/dalton

# Mono- and di-nuclear tris(pyrazolyl)borato-oxo-tungsten(v) complexes with phenolate ligands: syntheses and structures, and magnetic, electrochemical and UV/Vis/NIR spectroscopic properties

**Keira M. Stobie,[a] Zöe R. Bell,[a] Thomas W. Munhoven,[a] John P. Maher,[a] Jon A. McCleverty,*[a] Michael D. Ward,*[a] Eric J. L. McInnes,[b] Federico Totti[c] and Dante Gatteschi[c]**

[a] *School of Chemistry, University of Bristol, Cantock's Close, Bristol, UK BS8 ITS. E-mail: mike.ward@bristol.ac.uk*

[b] *EPSRC cwEPR Service Centre, Chemistry Department, University of Manchester, Manchester, UK M13 9PL*

[c] *Department of Chemistry, University of Florence, Via Maragliano 75/77, 50144, Florence, Italy*

***Received 29th August 2002, Accepted 25th October 2002***
***First published as an Advance Article on the web 27th November 2002***

A series of oxo-tungsten(v) complexes of the type [W(Tp*)(O)Cl(OAr)] (mononuclear) and [{W(Tp*)(O)Cl}$_2$(μ-OO)] (dinuclear, where 'OO' denotes a *para*-substituted bis-phenolate bridging ligand) has been prepared and many members structurally characterised. The complexes have been studied by a variety of physical techniques (electrochemistry; EPR spectroscopy; magnetic susceptibility; UV/Vis/NIR spectroelectrochemistry) in order to evaluate the electronic and magnetic interactions between the redox-active, paramagnetic metal centres and to compare the magnitudes of these interactions with those observed for the Mo(v) analogues. It was found that both electronic interactions (as measured by the separation between successive metal-centred redox processes) and magnetic exchange interactions (as determined from variable-temperature magnetic susceptibility studies) are reduced in the W(v) dinuclear complexes compared to their Mo(v) analogues, which we ascribe to a poorer d(π)–p(π) overlap between metal and bridging ligand orbitals. In addition the complexes have been fully characterised by UV/Vis/NIR spectroscopy in all accessible oxidation states, as well as by EPR spectroscopy.

## Introduction

The study of metal–metal interactions across bridging ligands in dinuclear complexes continues to be a subject which attracts a lot of interest, for two main reasons. Firstly, analysis of the spectroscopic behaviour of mixed-valence complexes provides a convenient way for testing our understanding of the process of electron-transfer in conditions where precise control of the parameters that affect it (distance, type of bridging pathway) is possible. Secondly, long-distance optically-induced electron-transfer is of interest as a simple model for electron transport in molecular electronic circuits, and studies on model mixed-valence dinuclear complexes allow the conductive properties of the bridging 'molecular wires' to be assessed.[1,2]

We have in the last few years studied electronic and magnetic coupling between metal centres in several series of dinuclear complexes,[3] prominent among which have been complexes of the type [{(Tp*)(O)(Cl)Mo$^{V}$}$_2$(μ-OO)], in which two tris(pyazolyl)-borato-oxo-molybdenum(v) units are connected by a bridging ligand ('OO') containing two phenolate termini. The significant electrochemical properties of these complexes may be summarised as follows.[3,4] Each metal centre undergoes (usually) chemically reversible Mo(v)/Mo(vi) and Mo(iv)/Mo(v) couples, such that the dinuclear complexes display two oxidations and two reductions with respect to the starting Mo(v)/Mo(v) state. In every case the redox separation between the two oxidations—typically, several hundred mV—is much greater than the redox separation between the two reductions, which are usually so close together as to be unresolved. This arises from participation of the HOMO of the bridging ligand in delocalisation of the oxidised Mo(v)/Mo(vi) mixed-valence state, such that metal-oxidised and ligand-oxidised forms are close in energy. This is in agreement with the known ability of *p*-bis-phenolates to be oxidised to semiquinones and then quinones and means that delocalisation can occur by hole-transfer [M$^+$–L–M ⟶ M–L$^+$–M ⟶ M–L–M$^+$]. In contrast the reduced Mo(iv)/Mo(v) mixed-valence state cannot undergo delocalisation by electron-transfer [M$^-$–L–M ⟶ M–L$^-$–M ⟶ M–L–M$^-$] because the bridging ligand LUMO is much higher in energy than the metal redox orbitals. A consequence of the proximity of the ligand HOMO to the metal redox orbitals is that in the oxidised Mo(v)/Mo(vi) and Mo(vi)/Mo(vi) forms of some of the complexes, very intense phenolate ⟶ Mo(vi) LMCT transitions occur in the near-IR region (1000–2000 nm) which make the complexes of interest as near-IR electrochromic dyes.[5]

The complexes [{(Tp*)(O)(Cl)Mo$^{V}$}$_2$(μ-OO)] have also been of interest because of their magnetic properties, with the sign of the magnetic exchange coupling constant between the two Mo(v) centres in the isovalent state being determined in a predictable manner by the topology of the bridging ligand; for example, *para*-substituted bridging ligands afford anti-ferromagnetic coupling whereas introduction of a *meta*-substitued connection affords ferromagnetic coupling, in agreement with a simple spin-polarisation picture for propagation of the exchange interaction.[3,6]

Having focused so extensively on molybdenum complexes because of their ideal properties (synthetic convenience, reversible redox behaviour, and the presence of strong electronic and magnetic interactions)[3–6] we have now extended our investigations into tungsten(v) chemistry—describing here a series of mononuclear and dinuclear complexes based on [(Tp*)W$^{V}$(O)-Cl(OAr)] units—for two reasons. Firstly, the expected differences between a second-row metal ion and its third row congener will have significant effects on the properties of the complexes. Lower ionisation potentials for third row metals will result in a shift in redox potentials such that oxidations are easier but reductions are more difficult; accordingly the energetic proximity of metal- and bridging-ligand based redox

DOI: 10.1039/b208397c

 

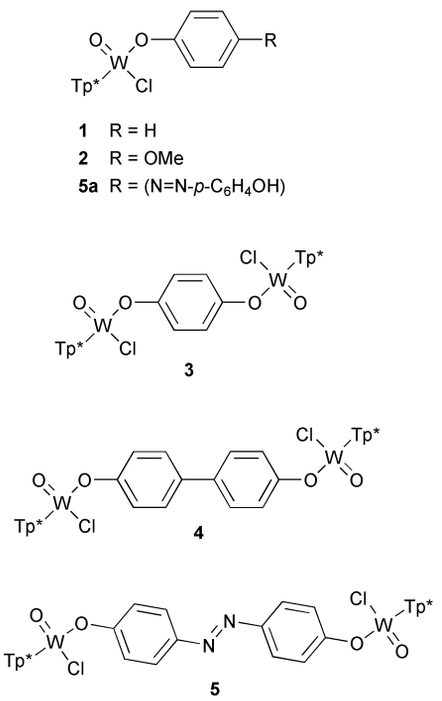


**Scheme 1** Structural formulae of the new complexes [Tp* = hydrotris(3,5-dimethylpyrazolyl)borate].

orbitals, which has such a strong influence on the chemistry of the oxo-Mo(v) complexes, will be affected. Also, the greater spatial extension of 5d orbitals compared to 4d will alter the interaction between metal and bridging-ligand orbitals and therefore affect the strengths of magnetic and electronic metal–metal interactions. Secondly, the +5 oxidation state of tungsten is much less well explored than the +4 and +6 oxidation states, so a fundamental electrochemical and spectroscopic study of such complexes is therefore of interest. We note that oxo- and thio-tungsten complexes with tris(pyrazolyl)borate ligands, with metal oxidation states of +4 to +6, have been studied by Young and co-workers,[7] in part because of their biological relevance.[8]

## Results and discussion

### Synthesis and characterisation

The complexes we have prepared are shown in Scheme 1, and are mononuclear complexes of the form [W(Tp*)(O)Cl-($OC_6H_4R$)] or dinuclear complexes of the form [{(Tp*)-(O)(Cl)$W^V$}$_2$(μ-OO)] ('OO' denoting, as mentioned above, a bridging ligand with two phenolate termini). They were prepared by reaction of the appropriate mono- or bis-phenol ligand (deprotonated with NaH) with [W(Tp*)(O)$Cl_2$] in anhydrous pyridine at reflux, in a similar manner to the molybdenum analogues.[4,6] However, long reaction times (several days) were necessary due to the kinetic inertness of the third-row metal precursor complex, and extensive column chromatography was necessary to separate the desired products from numerous by-products which formed. Complexes **1** and **2** are mononuclear complexes of phenol and 4-methoxyphenol, respectively; **3**–**5** are dinuclear complexes based on the bridging ligands 1,4-dihydroxybenzene, 4,4′-biphenol, and 4,4′-azophenol respectively. Complex **5a** is the mononuclear analogue of **5** arising from metallation at only one of the two phenol termini, and could be separated from the dinuclear complex by chromatography as it is more polar (with a free hydroxyl group) and hence elutes more slowly. Traces of the corresponding mononuclear complexes were also observed during chromatographic purification of **3** and **4** but these will not be further discussed here.

**Table 1** Selected bond distances (Å) for the new crystal structures

| | | | |
|---|---|---|---|
| [W(Tp*)$OCl_2$] | | | |
| W(1)–O(1) | 2.10(2) | W(1)–N(11) | 2.195(6) |
| W(1)–Cl(1) | 2.222(4) | W(1)–N(21) | 2.192(8) |
| W(1)–Cl(2) | 2.243(8) | | |
| Complex **1** | | | |
| W(1)–O(1) | 1.779(18) | W(1)–O(41) | 1.954(6) |
| W(1)–O(1′) | 1.992(14) | W(1)–N(12) | 2.225(7) |
| W(1)–Cl(1) | 2.209(8) | W(1)–N(32) | 2.227(8) |
| W(1)–Cl(1′) | 2.228(8) | W(1)–N(22) | 2.183(6) |
| Complex **2** | | | |
| W(1)–O(1) | 1.808(12) | W(1)–O(41) | 1.952(3) |
| W(1)–O(1′) | 1.839(12) | W(1)–N(11) | 2.223(4) |
| W(1)–Cl(1) | 2.221(4) | W(1)–N(21) | 2.240(3) |
| W(1)–Cl(1′) | 2.193(5) | W(1)–N(31) | 2.155(3) |
| Complex **3** | | | |
| W(1)–O(1) | 1.721(6) | W(1)–N(21) | 2.179(7) |
| W(1)–O(41) | 1.948(6) | W(1)–N(31) | 2.295(7) |
| W(1)–N(11) | 2.153(7) | W(1)–Cl(1) | 2.328(2) |
| Complex **5** | | | |
| W(1)–O(1) | 1.846(17) | W(1)–O(48) | 1.954(5) |
| W(1)–O(1′) | 1.952(14) | W(1)–N(22) | 2.147(5) |
| W(1)–Cl(1) | 2.187(4) | W(1)–N(12) | 2.225(5) |
| W(1)–Cl(1′) | 2.138(6) | W(1)–N(32) | 2.187(6) |
| Complex **5a** | | | |
| W(1)–O(1) | 1.896(6) | W(2)–O(148) | 1.951(6) |
| W(1)–O(48) | 1.954(6) | W(2)–O(2) | 2.094(5) |
| W(1)–N(11) | 2.164(6) | W(2)–N(131) | 2.148(7) |
| W(1)–N(21) | 2.164(8) | W(2)–Cl(2) | 2.184(4) |
| W(1)–Cl(1) | 2.281(3) | W(2)–N(121) | 2.195(7) |
| W(1)–N(31) | 2.286(6) | W(2)–N(111) | 2.242(7) |

The complexes were characterised by FAB mass spectroscopy and elemental analysis. The crystal structures were determined of the starting material [W(Tp*)(O)$Cl_2$] and of complexes **1**, **2**, **3**, **5** and **5a**; crystal and data collection parameters are summarised in Table 4 (see Experimental), and relevant bond lengths in Table 1. For [W(Tp*)(O)$Cl_2$] (Fig. 1)

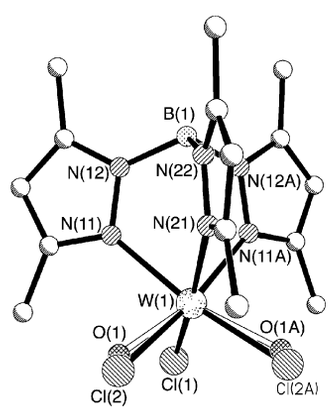


**Fig. 1** Molecular structure of [W(Tp*)(O)$Cl_2$].

the complex lies astride a mirror plane, such that the oxo ligand [O(1)] and one of the Cl ligands [Cl(2)] are disordered over two equivalent sites with 50 : 50 occupancy of each atom in each site. The other Cl ligand, Cl(1), is not disordered and lies in the mirror plane. The structure is generally similar to that of [Mo(Tp*)(O)$Cl_2$].[9]

The structures of complexes **1**, **2**, **3**, **5** and **5a** are shown in Figs. 2–6 respectively and largely speak for themselves. All have similar pseudo-octahedral coordination geometries at the metal centres, with **1**, **2** and **5** clearly exhibiting O/Cl disorder (it is shown for **1** and **2**, but not for **5** for the sake of clarity). For the remaining two complexes, there are significant differences between the respective W=O and W–Cl distances, with the W=

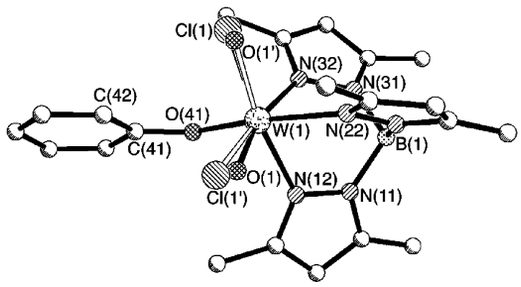


**Fig. 2** Molecular structure of complex **1**.

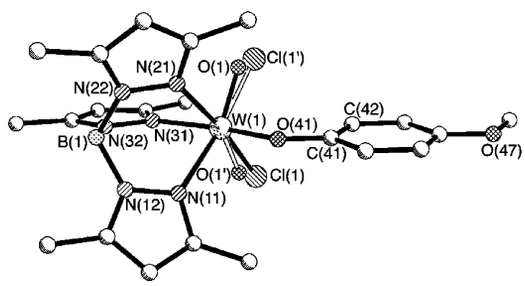


**Fig. 3** Molecular structure of complex **2**.

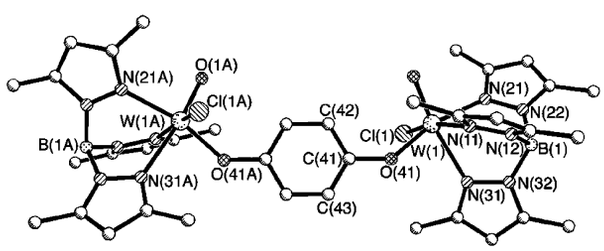


**Fig. 4** Molecular structure of complex **3**.

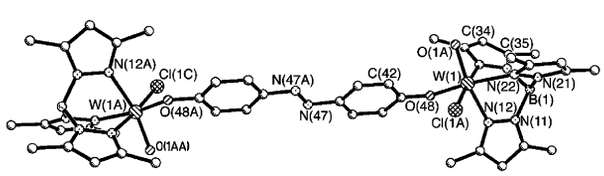


**Fig. 5** Molecular structure of complex **5**.

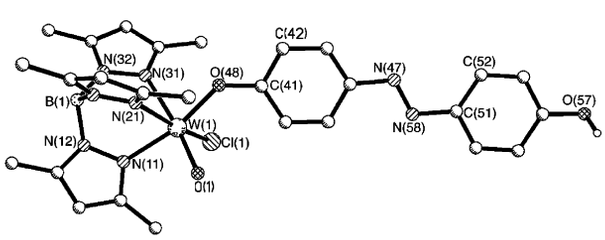


**Fig. 6** Molecular structure of complex **5a**. There are two independent molecules in the asymmetric unit of which only one is shown.

O distance being longer in **5a** than in **3** [1.896(6) *vs.* 1.721(6) Å] but the W–Cl distance being shorter [2.281(3) *vs.* 2.328(2) Å]. This is indicative of unresolved O/Cl disorder in **5a** which will tend to (apparently) lengthen the W=O bond but shorten the W–Cl bond; we have commonly seen this type of disorder in the Mo analogues.[4,6] For this reason the W=O and W–Cl distances in **3** [1.721(6) and 2.328(2) Å] are likely to be the most accurate, and the values observed are comparable to those for the corresponding oxo-Mo(v) complexes. In all cases the W–O(phenolate) distances are *ca.* 1.95 Å. There is a clear *trans*-influence of the strongly electron-donating oxo ligand, with the Mo–N bond in the *trans* position being significantly longer (*ca.* 2.3 Å in the complexes where there is not O/Cl disorder) than the W–N bonds which are *trans* to the phenolate or chloride ligands (<2.2 Å). In all cases, the orientation of the coordinated phenolate ring is such that the steric interaction with the two adjacent pyrazolyl methyl groups is minimised, which results in the phenolate ring being approximately coplanar with the pyrazolyl ring which is *trans* to it. In the dinuclear complexes **3** and **5**, both of which have twofold symmetry (a $C_2$ axis in the former and an inversion centre in the latter), the W ··· W separations are 8.34 and 14.69 Å. In **3** this is likely to be less than the solution separation, because the two W centres have a crystallographically-imposed *syn* disposition with respect to the bridging ligand, which will be relaxed in solution.

## Electrochemical properties

The electrochemical properties of **1**–**5** were examined by cyclic and Osteryoung square-wave voltammetry in $CH_2Cl_2$; the results are summarised in Table 2. It will be necessary to compare the redox behaviour of these complexes with that of their molybdenum analogues, and to simplify this we will abbreviate the Mo analogues of **1**–**5** as **1(Mo)**–**5(Mo)**, such that *e.g.* [Mo(Tp*)(O)Cl(OPh)] is **1(Mo)** and [{Mo(Tp*)(O)Cl}$_2$-(μ-1,4-$C_6H_4O_2$)] is **3(Mo)**.

Mononuclear complex **1** undergoes two reversible, one-electron redox processes at +0.13 and −1.75 V *vs.* the ferrocenium/ferrocene couple (hereafter abbreviated as $Fc^+$/Fc), which we assign as metal-centred W(VI)/W(V) and W(V)/W(IV) couples respectively. These may be compared with the Mo(VI)/Mo(V) and Mo(V)/Mo(IV) couples of **1(Mo)**, which occur at +0.68 and −1.21 V *vs.* $Fc^+$/Fc under the same conditions. The shift to more negative potential by *ca.* 550 mV of both redox processes on moving from Mo to W reflects the expected greater ease of oxidation of the third row metal ion (this is a uniform feature of all of these tungsten complexes with respect to their molybdenum analogues and it will be taken for granted in subsequent discussions).[7d] Complex **2**, with a methoxy substituent on the phenyl ring, behaves comparably [Fig. 7(a)], although the redox

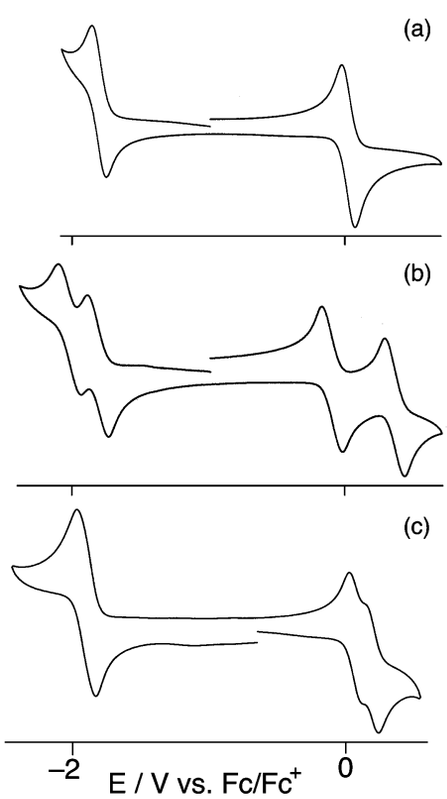


**Fig. 7** Cyclic voltammograms of (a) **2**, (b) **3** and (c) **4** in $CH_2Cl_2$.

**Table 2** Electrochemical data for the complexes

| Complex | Redox processes ($E_{1/2}$/V *vs.* $Fc^+/Fc$)[a] | | |
|---|---|---|---|
| | W(VI)/W(V) | W(V)/W(IV) | $\Delta E_{1/2}$[b]/mV |
| **1** | +0.13 (80)[c] | −1.75 (100) | — |
| **2** | +0.03 (100) | −1.80 (120) | — |
| **3** | +0.39 (90), −0.06 (90) | –1.78 (100), −1.99 (140) | 450 |
| **4** | +0.21 (100), +0.07 (100) | −1.75 (160)[d] | 140 |
| **5** | +0.27 (90), +0.16 (100) | −1.66 (170)[d,e] | 110 |

[a] Measured in $CH_2Cl_2$ containing 0.1 M $^nBu_4NPF_6$, at room temperature with a Pt-bead working electrode. Decamethylferrocene was used as an internal standard; potentials were then converted to the $Fc^+/Fc$ scale (redox potential for decamethylferrocene is −0.55 V *vs.* $Fc^+/Fc$ in $CH_2Cl_2$). [b] Separation between the two W(VI)/W(V) couples for the dinuclear complexes. [c] Figures in parentheses are peak–peak separations in mV recorded at a scan rate of 200 mV $s^{-1}$. [d] Two overlapping, unresolved W(V)/W(IV) couples giving a single broad, double-intensity wave by cyclic voltammetry. [e] Square-wave voltammetry showed two just-resolved maxima at −1.63 and −1.68 V.

potentials are slightly more negative, reflecting the electron-donating nature of the methoxy substituent which will further stabilise the higher oxidation states.

Dinuclear complex **3** shows four redox processes, all apparently chemically reversible; the two W(VI)/W(V) couples are at +0.39 and −0.06 V *vs.* $Fc^+/Fc$, and the two W(V)/W(IV) couples are at −1.78 and −1.99 V *vs.* $Fc^+/Fc$ [Fig. 7(b)]. The separation of 450 mV between the two W(VI)/W(V) couples indicates a strong electronic coupling in the +6/+5 mixed-valence state arising from delocalisation across the bridging ligand; the separation of 210 mV between the W(V)/W(IV) denotes a weaker, but still significant, interaction in the reduced +5/+4 mixed-valence state (the comproportionation constants are *ca.* $5 \times 10^7$ and $4 \times 10^3$ respectively). Complex **3** is therefore showing the same general behaviour as **3(Mo)**, with a stronger electronic interaction in the oxidised mixed-valence state than in the reduced mixed-valence state, for the reasons outlined earlier;[3] the fact that the bridging ligand is itself 'oxidisable' (*i.e.* has a high-energy HOMO) means that there will be a greater degree of ligand-centred character, and hence delocalisation, for the W(VI)/W(V) couples compared to the W(V)/W(IV) couples. An important difference however is that both redox separations in **3** (450 and 210 mV) are less than in **3(Mo)**, for which the separations between the two Mo(VI)/Mo(V) and the two Mo(V)/Mo(IV) couples are 990 and 250 mV respectively.[4c] The most obvious explanation for this is a smaller degree of W[d(π)]–O[p(π)] metal–ligand overlap arising from the greater spatial extension of the 5d orbitals on tungsten, such that *any* metal–metal electronic interaction (be it hole transfer in an oxidised mixed-valence state or electron-transfer in a reduced-mixed valence state) will be diminished.

Complexes **4** [Fig. 7(c)] and **5** show the same general pattern, although the redox splittings are reduced as the bridging ligands become longer. The separation between the W(VI)/W(V) couples is 140 mV across a biphenyl bridge in **4**, and 110 mV across a phenyl–azo–phenyl spacer (which is longer but more planar) in **5**. The relative ordering of these is the same as we observed for the analogous redox splittings in **4(Mo)** and **5(Mo)** (440 and 220 mV respectively),[4a] although again the interactions are weaker in the tungsten complexes. In both cases the two W(V)/W(IV) couples are so close together that they are not resolved by cyclic voltammetry, giving a broad, double-intensity wave, although square-wave voltammetry just reveals two closely-spaced maxima about 50 mV apart for **5**.

### Magnetic susceptibility studies

We performed variable-temperature magnetic susceptibility measurements on complexes **3**, **4** and **5** in order to compare the sign and strength of the spin-exchange interactions with those of their Mo(V) analogues **3(Mo)**, **4(Mo)** and **5(Mo)**. All three complexes show an antiferromagnetic coupling [for **3**: $J = -55$ $cm^{-1}$, $g = 1.80(2)$; for **4**, $J = -8.0(3)$ $cm^{-1}$, $g = 1.74(5)$; for **5**, $J = -10.7(7)$ $cm^{-1}$, $g = 1.87(8)$]. These may be compared with $J$ values of −80, −10 and −12.8 $cm^{-1}$ for the Mo analogues.[6c] There are three points to note about these data. Firstly, all coupling constants indicate intramolecular antiferromagnetic exchange, which is to be expected on the basis of the pattern of induced spins (from spin-polarisation) across *para*-substituted bridging ligands; this is in agreement with the properties of the Mo analogues.[4a,6c] Secondly, the couplings for **4** and **5** are much weaker than for **3**, as expected, because of the less effective pathway for magnetic exchange: the bridging ligands in **4** and **5** are longer than in **3**, and moreover for **4** there will be a twist between the phenyl rings which disrupts the necessary π-overlap.[6c] Finally, the magnitude of the coupling constants for **3**–**5** are all reduced compared to the values for **3(Mo)**–**5(Mo)** respectively. This can be ascribed to a less effective 5d–5d interaction with respect to the 4d–4d interaction. Evidence to support this hypothesis comes from comparison of the crystal structures of **3** and **3(Mo)**, which show that the geometric arrangement of metal fragments with respect to the bridging ligand is actually better optimised to promote magnetic exchange in **3** compared to **3(Mo)**;[10] accordingly, the efficiency of the superexchange pathway should be enhanced for **3** compared to **3(Mo)**. Nevertheless, we find a weaker magnetic interaction, confirming the less effective 5d–5d interaction through such a π-system which presumably arises from poorer overlap of the 5d orbitals with the π-system of the bridging ligand. The same conclusion was reached above on the basis of electrochemical data.

### EPR spectra

The EPR spectrum of **1** in fluid solution shows a resonance at $g_{av} = 1.79$. At X-band frequency the expected satellites, arising from coupling to $^{183}W$ ($I = 1/2$, 14.3% natural abundance), are barely visible as shoulders on the main signal. However, the satellites are much more clearly resolved by changing frequency to S-band and by lowering the temperature to 200 K [Fig. 8(a)], and under these conditions the hyperfine coupling is 100 G. On freezing the solution (110 K) a rhombic spectrum appears, which is best resolved at X-band [Fig. 8(b)]. Hyperfine satellites are visible on all three components of the signal, and the EPR spectral parameters (confirmed by simulation) are as follows: $g_1 = 1.849$ ($A_1 = 100$ G); $g_2 = 1.811$ ($A_2 = 75$ G); $g_3 = 1.731$ ($A_3 = 133$ G), with Gaussian linewidths of 19, 21 and 19 G respectively. The low $g$-values (less than the free-spin value, $g_e = 2.0023$) are characteristic of mono-oxo metal centres with a $(d_{xy})^1$ electron configuration;[11] that they are lower than the values associated with analogous oxo-Mo(V) complexes[4,6] is due to the greater spin–orbit coupling of W. The average $g$ and $A$ values derived from these agree well with the values obtained from the isotropic spectrum. There are few published EPR spectra of W(V) complexes,[12] and the spectrum of **1** corresponds most closely to that of *cis*-$[W(O)Cl(hq)_2]$ (Hhq = 8-hydroxyquinoline).[12b] The spectra of the other mononuclear complexes (**2**, **5a**) are essentially identical to that of **1**.

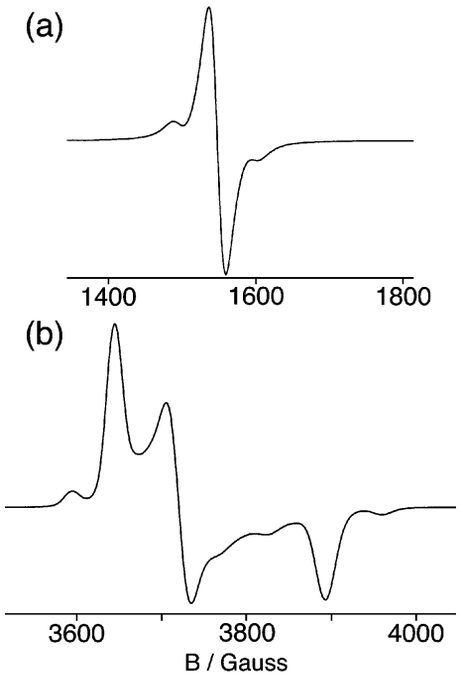


**Fig. 8** EPR spectra of complex **1** in $CH_2Cl_2$–thf: (a) S-band at 200 K; (b) X-band at 110 K.

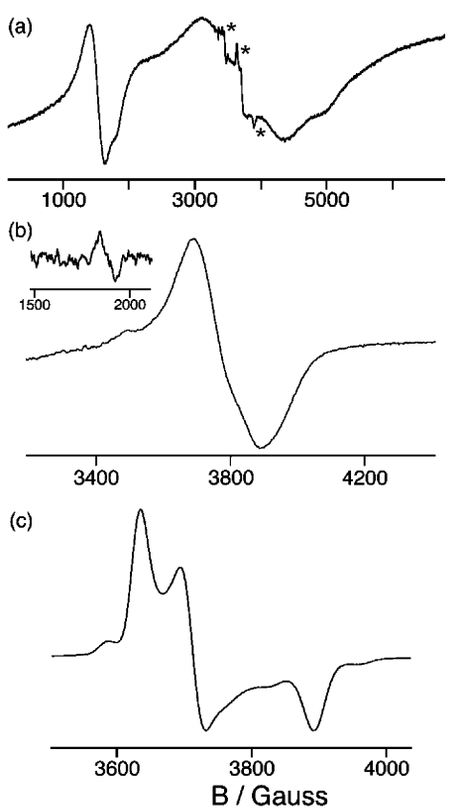


**Fig. 9** X-Band EPR spectra of (a) **3**, (b) **4** and (c) $[\mathbf{3}]^+$ in $CH_2Cl_2$–thf at 90 K. In part (a), the small, sharp features labelled * arise from aerial oxidation to give traces of $[\mathbf{3}]^+$; these features correspond exactly to those in part (c).

The frozen-solution X-band spectrum of dinuclear complex **3** [Fig. 9(a)] is completely different, consisting of a very broad main signal centred at around $g = 1.80$ with a peak–peak separation of *ca.* 1300 G. Superimposed on this are weak, relatively sharp features (labelled * in the figure) which arise from a trace of aerial oxidation to give the mono-oxidised W(V)–W(VI) complex whose spectrum is that of an isolated W(V) centre like that in Fig. 8 (see later for discussion of the mixed-valence complex); the underlying spectrum of the triplet is however characteristically broad and featureless due to exchange broadening. A strong, narrower signal at $g = 4.42$ is a rather intense $\Delta m_s = 2$ ('half-field') signal associated with simultaneous flipping of both electron spins. The spectrum of **3** is similar to that observed for **3(Mo)**,[4c] with the variations that (i) the signal is very much broader (a phenomenon which has been noted before when comparing EPR spectra of Mo and W analogues),[12b] and (ii) the intensity of the $\Delta m_s = 2$ signal with respect to the main signal is much higher. Using the parameters of this spectrum (specifically, the position of the $\Delta m_s = 2$ signal, and its intensity with respect to the $\Delta m_s = 1$ signal; and the spread of the components of the $\Delta m_s = 1$ signal), simulation allowed the zero-field splitting in **3** to be determined as $\leq 0.11$ cm$^{-1}$. As the two metal centres become further apart from one another in **4**, the frozen-solution spectrum becomes narrower ($g = 1.78$; peak–peak separation about 150 G) but is still fairly featureless; the $\Delta m_s = 2$ signal at $g = 4.25$ is reduced in intensity to the extent that it is only just detectable. Simulation of this spectrum shows that the zero-field splitting of **4** is $\leq 0.01$ cm$^{-1}$, an order of magnitude weaker than in **3**, in agreement with the weaker antiferromagnetic exchange interaction for **4** as described earlier. The spectrum of **5** under the same conditions is similar to that of **4**.

Given the separation of 450 mV between the two successive W(V)/W(VI) couples of complex **3**, the mono-oxidised W(V)–W(VI) mixed-valence complex could be generated by chemical oxidation simply by addition of ferrocenium hexafluorophosphate to a sample in an EPR tube [the first W(V)/W(VI) couple occurs at −0.06 V *vs.* $Fc/Fc^+$]. The frozen-solution spectrum of this sample at 90 K is essentially identical to that of mononuclear complex **1** [Fig. 8(b)]; the $g$ and $A$ values are the same within the error limits of the measurement. This indicates that the unpaired electron is localised at one terminus giving chemically distinct W(V) and W(VI) termini; this is not surprising in a frozen glass, given that the solvent repolarisation which accompanies electron transfer in solution is prevented. In fluid solution at 200 K the spectrum of $[\mathbf{3}]^+$ is again identical to that of **1**, (in particular, the intensities of the hyperfine satellites), indicating valence localisation under these conditions also;[13] more precisely, any delocalisation arising from back-and-forth electron transfer between the termini is slower than the EPR timescale. The presence of a significant degree of electronic coupling from the electrochemical data, combined with the observation of localised valences on the EPR timescale means that $[\mathbf{3}]^+$ is a class II mixed-valence species. On this basis the mixed-valence species $[\mathbf{4}]^+$ and $[\mathbf{5}]^+$, with a weaker electronic interaction compared to $[\mathbf{3}]^+$, will certainly also be valence localised.

### UV/Vis/NIR spectroelectrochemistry

Several of the complexes were investigated by UV/Vis/NIR spectroelectrochemistry in $CH_2Cl_2$ solution in an OTTLE cell at 243 K; the results are summarised in Table 3.

**(i) Mononuclear complexes.** For mononuclear complex **1**, the electronic spectral features associated with transitions between the frontier orbitals may be assigned by analogy with **1(Mo)**, taking account of the expected higher energy of the tungsten 5d orbitals compared to molybdenum 4d. Thus, the lowest energy transition at 424 nm is ascribed to a phenolate → W(V) LMCT transition, occurring at a higher energy than the related transition in **1(Mo)**. On oxidation to the W(VI) state, this LMCT transition is red-shifted to 490 nm, because the metal 5d orbital is lowered in energy on oxidation; and it becomes about five times more intense, because the receiving d-orbital is now completely empty so the transition dipole moment is increased. This is exactly in agreement with the behaviour of **1(Mo)** on oxidation.[4b]

**Table 3** Electronic spectral data from OTTLE experiments ($CH_2Cl_2$, 243 K)

| Complex | $n$ | $\lambda_{max}$/nm ($10^{-3}\varepsilon$/$M^{-1}$ $cm^{-1}$) |
|---|---|---|
| $[\mathbf{1}]^{n+}$ | 1− | 268 (6.4), 348 (sh), 446 (3.0) |
| | 0 | 237 (12), 295 (sh), 335 (sh), 425 (1.0) |
| | 1+ | 293 (7.6), 490 (6.3) |
| $[\mathbf{2}]^{n+}$ | 1− | 281 (6.6), 348 (sh), 446 (3.6) |
| | 0 | 236 (19), 296 (9.8), 345 (sh), 470 (2.0) |
| | 1+ | 275 (11), 390 (5.8), 623 (16) |
| $[\mathbf{3}]^{n+}$ | 2− | 301 (11), 456 (6.6) |
| | 1− | 298 (10), 358 (sh), 455 (4.0), 550 (2.7) |
| | 0 | 236 (31), 301 (13), 348 (sh), 517 (4.6) |
| | 1+ | 245 (sh), 286 (13), 730 (7.7) |
| | 2+ | 296 (17), 398 (10), 595 (19) |
| $[\mathbf{4}]^{n+}$ | 2− | 303 (24), 465 (13) |
| | | 238 (33), 305 (31), 335 (sh), 385 (sh), 491 (4.9) |
| | 1+ | 246 (sh), 300 (21), 361 (sh), 440 (6.5), 738 (10) |
| | 2+ | 255 (36), 298 (sh), 372 (sh), 640 (26) |
| $[\mathbf{5}]^{n+}$ | 2− | 299 (sh), 414 (27), 446 (sh), 681 (10), 893 (10) |
| | 1− | 292 (21), 414 (19), 446 (sh), 690 (4.0), 898 (4.0) |
| | 0 | 236 (34), 291 (sh), 374 (24), 458 (24) |
| | 1+ | 292 (sh), 372 (20), 442 (20), 664 (11) |
| | 2+ | 318 (22), 378 (sh), 615 (24) |
| $[\mathbf{5a}]^{n+}$ | 2− | 315 (6.6), 414 (sh), 461 (17), 653 (3.6), 823 (2.6) |
| | 1− | 240 (19), 305 (7.3), 416 (15), 443 (15) |
| | 0 | 242 (20), 298 (sh), 349 (sh), 368 (22), 400 (sh), 433 (14) |
| | 1+ | 245 (sh), 287 (sh), 359 (16), 643 (12) |

On one-electron reduction to the W(IV) state there are two significant changes to the spectrum. Firstly, a weak transition at *ca.* 800 nm is the expected[4b] d–d transition occurring within the non-degenerate d(π) orbital set, arising from the $(d_{xy})^2(d_{xz})^0(d_{yz})^0$ configuration (the $d_{xz}$ and $d_{yz}$ orbitals are raised in energy by the π-donor oxo ligand, and therefore are not of pure d-character, allowing the 'forbidden' transition to gain intensity). Secondly, a relatively intense transition at 446 nm occurs which is not present for $[\mathbf{1(Mo)}]^-$; it is to be expected that the phenolate ⟶ W(V) LMCT transition of **1** will collapse on reduction of the metal, leaving this region of the spectrum empty. The nature of this transition in $[\mathbf{1}]^-$ is not immediately obvious. It is too intense to be a d–d transition, and too low in energy (and too weak) to be a ligand-centred π–π* transition. The fact that it appears only when the metal is reduced suggests that it is an MLCT process; the only plausible π-acceptor ligand is the Tp* which, although anionic, has three aromatic rings which each contain two electronegative atoms. Accordingly this transition is assigned as a W(IV) ⟶ pyrazolyl(π*) MLCT process. In **1(Mo)** this would also be expected, but at higher energy because of the lower energy of the Mo[d(π)] orbital set, and therefore obscured by the ligand-centred transitions in the UV region. Thus, its appearance when W(V) is reduced to W(IV), and the fact that a similar transition is not apparent in the same part of the spectrum for $[\mathbf{1(Mo)}]^-$, are both in agreement with its assignment as W(IV) ⟶ pyrazolyl(π*) MLCT.

The behaviour of **2** is generally similar (Fig. 10): the phenolate ⟶ W(V) LMCT transition ($\lambda_{max}$ = 470 nm; $\varepsilon$ = 2000 $M^{-1}$ $cm^{-1}$) becomes, on oxidation to $[\mathbf{2}]^+$, a more intense and lower energy phenolate ⟶ W(VI) LMCT transition ($\lambda_{max}$ = 623 nm; $\varepsilon$ = 16000 $M^{-1}$ $cm^{-1}$); and is replaced, on reduction to $[\mathbf{2}]^-$ by a W(IV) ⟶ pyrazolyl(π*) MLCT transition ($\lambda_{max}$ = 446 nm; $\varepsilon$ = 3600 $M^{-1}$ $cm^{-1}$).

**(ii) Dinuclear complexes.** The electronic spectra of **3** were studied in all five accessible oxidation states from $[\mathbf{3}]^{2-}$ [W(IV)-W(IV)] to $[\mathbf{3}]^{2+}$ [W(VI)-W(VI)] (Fig. 11), and can be interpreted with reference to the spectra of the mononuclear complexes (above). For **3** in the W(V)–W(V) state, the (bridging ligand) ⟶ W(V) LMCT transition is at 517 nm, slightly red-shifted compared to the mononuclear complexes, because the HOMO of the bridging ligand $[OC_6H_4O]^{2-}$ will be higher in energy than

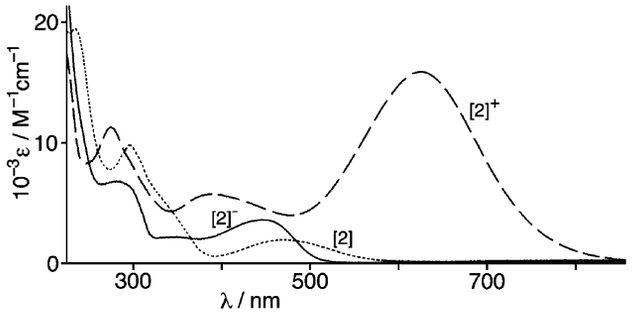


**Fig. 10** Electronic spectra ($CH_2Cl_2$, 243 K) of $[\mathbf{2}]^{n+}$ ($n$ = −1, 0, +1).

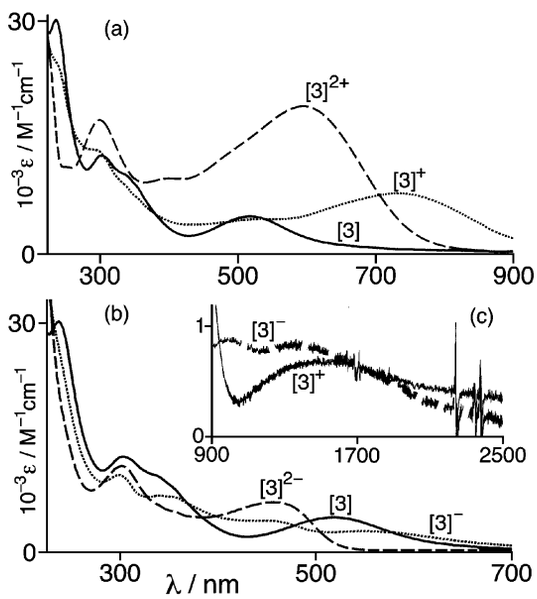


**Fig. 11** Electronic spectra ($CH_2Cl_2$, 243 K) of $[\mathbf{3}]^{n+}$: (a) $n$ = 0, +1, +2; (b) $n$ = 0, −1, −2. Part (c) shows the IVCT transitions in the NIR region for $n$ = +1 and −1.

that of phenolate due to the double negative charge, and consequently nearer in energy to the metal d(π) orbitals. One-electron oxidation to $[\mathbf{3}]^+$ [Fig. 11(a)] produces the expected lower energy and more intense (bridging ligand) ⟶ W(VI) LMCT transition ($\lambda_{max}$ = 730 nm; $\varepsilon$ = 7700 $M^{-1}$ $cm^{-1}$); this is blue shifted and gains in intensity slightly following the second oxidation to $[\mathbf{3}]^{2+}$ ($\lambda_{max}$ = 595 nm; $\varepsilon$ = 19000 $M^{-1}$ $cm^{-1}$). It is clear from this behaviour that the two metal centres are not electronically independent, or this transition in $[\mathbf{3}]^{2+}$ would be at the same energy as in $[\mathbf{3}]^+$ but with double the intensity. Instead, the second oxidation ($[\mathbf{3}]^+ \longrightarrow [\mathbf{3}]^{2+}$) appears to stabilise the bridging ligand orbitals such that the LMCT process in $[\mathbf{3}]^{2+}$ is blue-shifted compared to that in $[\mathbf{3}]^+$.

Successive reduction of **3** to $[\mathbf{3}]^-$ and then $[\mathbf{3}]^{2-}$ [Fig. 11(b)] results in steady replacement of the (bridging ligand) ⟶ W(V) LMCT transition by the W(IV) ⟶ pyrazolyl(π*) MLCT transition at higher energy. In the W(V)/W(IV) state for $[\mathbf{3}]^-$ both can be seen, the former at 565 nm with an intensity reduced by about 50% compared to **3**, and the latter at 455 nm ($\varepsilon$ = 3200 $M^{-1}$ $cm^{-1}$). On further reduction to $[\mathbf{3}]^{2-}$, the LMCT transition associated with W(V) disappears and the MLCT transition associated with W(IV) ($\lambda_{max}$ = 456 nm; $\varepsilon$ = 6600 $M^{-1}$ $cm^{-1}$) gains in intensity, as expected.

These features of the electronic spectra of **3** and its redox partners in the UV/Vis region are clearly related to those of the mononuclear complexes **1** and **2**. In the near-IR region however, additional transitions occur for $[\mathbf{3}]^+$ and $[\mathbf{3}]^-$, both mixed-valence complexes, which do not occur for mononuclear **1** and **2**, and do not occur for the isovalent dinuclear species $[\mathbf{3}]^{2-}$, **3** and $[\mathbf{3}]^{2+}$. For both $[\mathbf{3}]^+$ and $[\mathbf{3}]^-$ there is a broad transi-

tion at *ca.* 1400 nm with an intensity of *ca.* 1000 $M^{-1}$ $cm^{-1}$, which are assigned as W(V) ⟶ W(VI) and W(IV) ⟶ W(V) intervalence charge-transfer transitions, respectively. These are not very well resolved, and the spectrum of $[\mathbf{3}]^-$ appears to have at least two components, but it is clear that the widths of these signals are consistent with class II mixed-valence character in each case.

For the dinuclear complex **4**, with an additional phenyl spacer in the bridging ligand, the evolution of spectra in the different oxidation states (Fig. 12) is comparable to that of **3**,

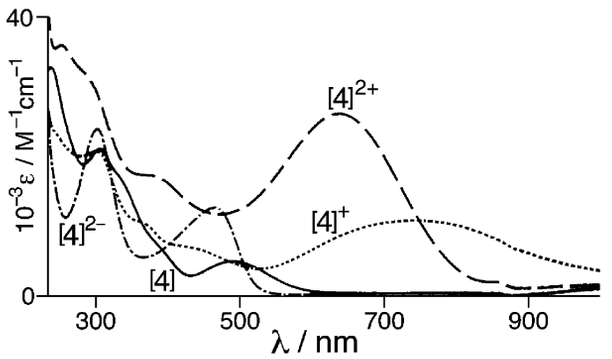


**Fig. 12** Electronic spectra ($CH_2Cl_2$, 243 K) of $[\mathbf{4}]^{n+}$ ($n$ = −2, 0, +1, +2).

with two exceptions. Firstly, the fact that the two W(V)/W(IV) couples are almost coincident means that it was not possible to electrochemically generate mono-reduced $[\mathbf{4}]^-$ and record its spectrum; reduction of **4** proceeded directly to $[\mathbf{4}]^{2-}$. Secondly, we could find no evidence for IVCT transitions in the near-IR region, presumably because the reduced electronic coupling arising from the extended, twisted bridging ligand (compared to **3**)—which is obvious from the voltammetric data—makes any IVCT transitions too weak to detect. Apart from these limitations, the now-familiar spectroscopic behaviour is apparent. The characteristic phenolate ⟶ W(V) LMCT transition of **4** is the lowest energy transition ($\lambda_{max}$ = 491 nm; $\varepsilon$ = 4900 $M^{-1}$ $cm^{-1}$); oxidation to $[\mathbf{4}]^+$ affords the more intense and lower energy phenolate⟶ W(VI) LMCT transition ($\lambda_{max}$ = 738 nm; $\varepsilon$ = 10000 $M^{-1}$ $cm^{-1}$), which gains intensity and is blue-shifted on further oxidation to $[\mathbf{4}]^{2+}$ ($\lambda_{max}$ = 640 nm; $\varepsilon$ = 26000 $M^{-1}$ $cm^{-1}$). On reduction of **4** to $[\mathbf{4}]^{2-}$, the W(IV) ⟶ pyrazolyl(π*) MLCT transition appears at a similar position to those in the spectra of the reduced forms of **1**–**3** ($\lambda_{max}$ = 465 nm; $\varepsilon$ = 13000 $M^{-1}$ $cm^{-1}$). It is clear that in **4**, as in **3**, all of the redox processes are substantially metal-centred.

Complex **5** behaves somewhat differently due to the presence of the azo unit in the bridging ligand which makes the bridging ligand planar and lowers the energy of its orbitals. Consequently the spectrum of **5** is dominated by a series of intense transitions at around 400 nm which are associated with the bridging ligand; the free 4,4′-azophenol ligand has its principal π ⟶ π* transition at 351 nm in $CH_2Cl_2$ ($\varepsilon$ *ca.* 20000 $M^{-1}$ $cm^{-1}$) and a weaker n ⟶ π* transition at 421 nm ($\varepsilon$ *ca.* 1200 $M^{-1}$ $cm^{-1}$) which will be red-shifted on deprotonation. Accordingly the expected phenolate ⟶ W(V) LMCT transition of **5**, which occurs at *ca.* 500 nm for **3** and **4**, is not clearly resolved.

Successive oxidation of **5** to $[\mathbf{5}]^+$ and $[\mathbf{5}]^{2+}$ [Fig. 13(a)] generates the expected intense phenolate ⟶ W(VI) LMCT transitions at 664 and 615 nm respectively, with the intensity of this transition approximately doubling as the second W(VI) centre is generated. From this it is apparent that, as with the other tungsten complexes, the two oxidations are metal-based and accurately described as W(V)/W(VI) processes. This contrasts with the behaviour observed for the analogous molybdenum complex **5(Mo)**, for which—according to the UV/Vis/NIR spectroelectrochemistry—the doubly oxidised form has

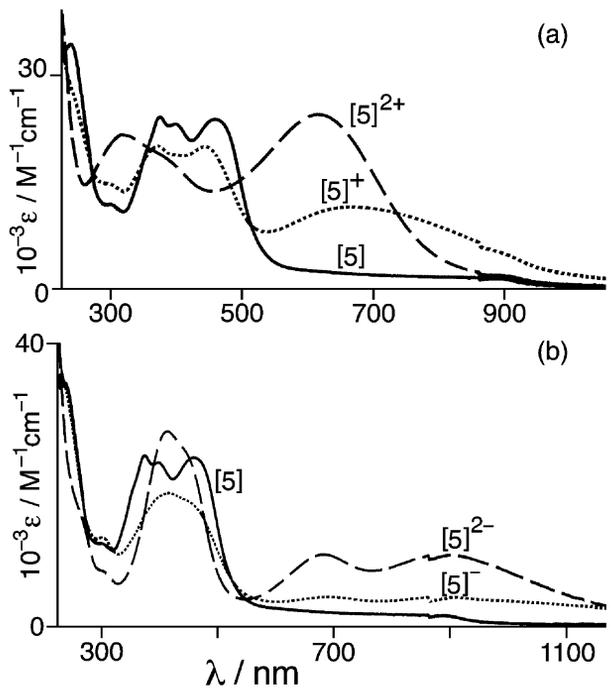


**Fig. 13** Electronic spectra ($CH_2Cl_2$, 243 K) of $[\mathbf{5}]^{n+}$: (a) $n$ = 0, +1, +2; (b) $n$ = 0, −1, −2.

undergone oxidation of the bridging ligand, to give a quinonoidal bridge between two Mo(V) centres.[4a] In **5**, the less positive redox potentials of the tungsten-based couples means that the ambiguity between metal- and ligand-centred oxidation is removed, with the metal centres clearly oxidising first.

On reduction to $[\mathbf{5}]^-$ and then $[\mathbf{5}]^{2-}$, two new transitions appear [Fig. 13(b)] which again are approximately twice as intense for $[\mathbf{5}]^{2-}$ than for $[\mathbf{5}]^-$, indicative of a simple additive affect arising from only weak electronic coupling between the centres (as shown by the voltammetric data). The higher-energy of these, at 690 nm for $[\mathbf{5}]^-$ and 681 nm for $[\mathbf{5}]^{2-}$, can be ascribed to the W(IV) ⟶ pyrazolyl(π*) MLCT transition in each case, although it is at rather lower energy than was seen for the reduced forms of **1**–**4**. The second new transition, at 898 and 893 nm for $[\mathbf{5}]^-$ and $[\mathbf{5}]^{2-}$ respectively, has no counterpart in any of the other spectra of reduced complexes described above, and for this reason we tentatively ascribe it to a W(IV) ⟶ azo(π*) MLCT transition involving the central electron-accepting NN unit of the bridging ligand. The relative ordering of these two MLCT transitions indicates that the π* orbital of the azo unit is below that of the pyrazolyl rings, in agreement with numerous electrochemical studies which show that azo-based ligands are particularly easy to reduce. Finally, we note that although clearly-defined IVCT transitions are not apparent for the mixed-valence species $[\mathbf{5}]^+$ and $[\mathbf{5}]^-$, the spectra of these complexes have low-energy tails which extend further into the near-IR region than do those of the isovalent complexes **5**, $[\mathbf{5}]^{2+}$ and $[\mathbf{5}]^{2-}$. This can be ascribed to the presence of unresolved, weak IVCT transitions for $[\mathbf{5}]^+$ and $[\mathbf{5}]^-$; that these are present for the mixed-valence forms of **5**, but not for **4**, is in agreement with the voltammetric data which show slightly stronger electronic interactions in **5**.

## Conclusions

A series of complexes of the type $[W^V(Tp^*)(O)Cl(OAr)]$ (mononuclear) and $[\{W(Tp^*)(O)Cl\}_2(\mu\text{-}OO)]$ (dinuclear, where 'OO' denotes a *para*-substituted bis-phenolate bridging ligand) has been prepared and many members structurally characterised. Each metal centre undergoes reversible W(IV)/W(V) and W(V)/W(VI) couples at potentials several hundred mV less

positive than the analogous oxo-Mo(v) complexes. The mononuclear complexes have two reversible redox interconversions and the dinuclear complexes have four, with the separation between successive W(v)/W(vi) couples always being larger than the separation between the W(iv)/W(v) couples, behaviour which is exactly comparable to the analogous oxo-Mo(v) complexes. The metal–metal electronic interactions as measured by the redox separation between successive W(v)/W(vi) couples are, however, considerably reduced compared to those in the oxo-Mo(v) analogues, which we ascribe to the poorer interaction of the bridging ligand orbitals with 5d compared to 4d metal orbitals; the oxidised mixed-valence W(v)–W(vi) complexes are valence-trapped on the EPR timescale. The same reduction of metal–metal communication in the dinuclear complexes is also apparent in the reduced antiferromagnetic coupling constants compared to the oxo-Mo(v) analogues. The complexes were further analysed by EPR spectroscopy and UV/Vis/NIR spectroelectrochemistry.

## Experimental

### Instrumental details

Fast Atom Bombardment (FAB) mass spectra were recorded on a VG-Autospec instrument using 3-nitrobenzyl alcohol as matrix; IR spectra were recorded on a Perkin-Elmer Spectrum One spectrophotometer. UV/Vis/NIR spectroelectrochemical measurements in $CH_2Cl_2$ at 243 K were recorded as descrbed previously, using a home-built OTTLE cell mounted in the sample compartment of a Perkin-Elmer Lambda 19 spectrophotometer.[14] All processes were checked for chemical reversibility by reversing the applied potential and ensuring that the starting spectrum could be regenerated. Electrochemical measurements were carried out with a PC-controlled EG&G-PAR 273A potentiostat connected to a standard three-electrode cell; ferrocene or decamethylferrocene was added at the end of each measurement as an internal reference, and all potentials are quoted *vs.* the ferrocene/ferrocenium couple which is taken as 0.0 V.

EPR spectra were recorded on a Bruker ESP-300E spectrometer, at either S-band (EPSRC cw-EPR service centre, University of Manchester) or X-band (University of Bristol); magnetic fields and microwave frequencies were measured with a Bruker ER035M Gaussmeter and an EIP model 588C microwave counter, respectively.

Magnetic susceptibilities were measured in the temperature range of 2–250 K in an applied field of 1 T using a Metronique Ingéniérie MS03 SQUID magnetometer; diamagnetic corrections were estimated from Pascal's constants.[15] The parameters $J$ and $g$ were obtained using the exchange spin Hamiltonian $H = -J\boldsymbol{S}_1\cdot\boldsymbol{S}_2$ (with positive $J$ indicating ferromagnetism and negative $J$ indicating antiferromagnetism).

### Syntheses

All of the following syntheses were carried out in dried, degassed solvents under a dinitrogen atmosphere.

**[W(Tp*)(O)Cl$_2$].** This preparation is based on a published method.[16] Allyltrimethylsilane (8.0 cm$^3$, 50.43 mmol) was slowly added to a solution of $WCl_6$ (5.00 g, 12.61 mmol) in dry diethyl ether (35 cm$^3$) under $N_2$. The mixture was stirred (90 mins) during which time a precipitate formed. The mother liquor was removed and cooled (0 °C) before dry THF (10 cm$^3$) was added, producing a cream precipitate. This mixture was stirred for 30 min before being allowed to warm to room temperature. Stirring was continued for a further 2 h during which time the initial precipitate redissolved into the brown solution, and a green solid appeared. The mother liquor was removed and the remaining green solid was washed with dry diethyl ether (5 × 10 cm$^3$). This solid was then suspended in dry THF (20 cm$^3$); KTp* (4.236 g, 12.61 mmol) was added, and the dark blue mixture was heated to reflux for 72 h. Evaporation of the solvent left a blue–purple solid which was purified by column chromatography (silica, $CH_2Cl_2$), with the desired product eluting first as a blue band (yield: 0.713 g, 10%). Spectroscopic and analytical data were consistent with those reported previously.[16]

**[W(Tp*)(O)Cl(OPh)] (1).** A mixture of phenol (0.066 g, 0.704 mmol) and [W(Tp*)(O)Cl$_2$] (0.200 g, 0.35 mmol) in dry pyridine (25 cm$^3$) was heated to reflux overnight. Sodium hydride (60% w/w dispersion in mineral oil; 0.0282 g, 0.70 mmol) was then added, instantly producing a purple solution. This solution was heated to reflux for four days, during which time it became green–brown in colour. After 4 days at reflux the solvent was removed to leave a green solid which was then purified by column chromatography on alumina using $CH_2Cl_2$–hexane (1 : 4, v/v) as eluent. The product was eluted as the first (green) band (yield: 0.0607 g, 28%), which was closely followed by a blue band of unreacted starting material. IR (KBr disc): $\nu$(B–H) 2546, $\nu$(Pz ring) 1539, $\nu$(W=O) 957 cm$^{-1}$. Anal. calc. for $C_{21}H_{27}N_6BClO_2W$: C, 40.3; H, 4.3; N, 13.4. Found: C, 40.0; H, 4.7; N, 13.7%. FABMS: *m*/*z* 648 (10%, $\{M + Na\}^+$, 625 (80%, $M^+$), 590 (10%, $\{M - Cl\}^+$).

**[W(Tp*)(O)Cl(OC$_6$H$_4$OCH$_3$)] (2).** A mixture of 4-methoxyphenol (0.0208 g, 0.17 mmol) and sodium hydride (60% w/w dispersion in mineral oil; 0.0134 g, 0.34 mmol) in dry pyridine (25 cm$^3$) was heated to reflux for 30 min, forming a yellow solution. After cooling to room temperature, [W(O)(Tp*)Cl$_2$] (0.200 g, 0.35 mmol) was added, resulting in a blue solution. This was again heated to reflux for 2 days, by which time the solution was a red–brown colour. After removal of the solvent the brown solid was purified by column chromatography on flash silica, using a gradient elution system starting with $CH_2Cl_2$–hexane (3 : 2) and then moving to MeCN–$CH_2Cl_2$ (1 : 19). The first (blue) band was unreacted starting material, the second (red–orange) band corresponded to the expected product (eluted with $CH_2Cl_2$); this fraction sometimes required further purification on another column (silica, $CH_2Cl_2$). Final yield: 0.0821 g, 74%. IR (solid): $\nu$(B–H) 2548, $\nu$(Pz ring) 1542, $\nu$(W=O) 953 cm$^{-1}$. Anal. calc. for $C_{22}H_{29}N_6BClO_3W$: C, 40.3; H, 4.4; N, 12.8. Found: C, 39.5; H, 5.0; N, 12.3%. FABMS: *m*/*z* 678 (5%, $\{M + Na\}^+$, 656 (100%, $\{M + H\}^+$), 620 (10%, $\{M - Cl\}^+$), 533 (20%, $\{M - OC_6H_4OMe\}^+$).

**[{W(O)(Tp*)Cl}$_2$(μ-OC$_6$H$_4$O)] (3).** A mixture of hydroquinone (0.0220 g, 0.20 mmol) and sodium hydride (60% w/w dispersion in mineral oil; 0.0160 g, 0.40 mmol) dissolved in dry pyridine (20 cm$^3$) was heated to reflux for 30 min to give a pale green–yellow solution. After cooling to room temperature, [W(O)(Tp*)Cl$_2$] (0.250 g, 0.44 mmol) was added, and the mixture was again heated to reflux for 3 days, during which time the solution darkened and became purple in colour. Removal of the solvent afforded a purple solid, which was purified by column chromatography on flash silica. Initial elution with $CH_2Cl_2$–hexane (3 : 2) resulted in elution of traces of blue starting material, followed by the desired dinuclear complex (purple). As solvent polarity was increased to $CH_2Cl_2$–thf (99 : 1), a further brown band eluted which was the mononuclear product, [W(O)(Tp*)Cl(OC$_6$H$_4$OH)] (identified on the basis of its FAB mass spectrum). Further purification of **3** on another column (flash silica, $CH_2Cl_2$) afforded the pure product. Final yield: (0.041 g, 17%). The complex decomposes slowly in solution and during chromatography, but rapid flash chromatography worked well. IR (solid): $\nu$(B–H) 2548, $\nu$(Pz ring) 1542, and $\nu$(W=O) 953 cm$^{-1}$. Anal. calc. for $C_{36}H_{48}N_{12}W_2B_2Cl_2O_4\cdot(C_6H_{14})_{0.5}$: C, 38.5; H, 4.5; N, 13.8. Found: C, 38.2; H, 4.3; N, 13.6%. FABMS: *m*/*z* 1172 (100%, $M^+$).

**Table 4** Crystallographic data[a]

| Compound | $[W(Tp^*)OCl_2]$ | **1** | **2** | **3**·$(C_6H_{14})(C_5H_{12})$ | **5**·$(Et_2O)_2$ | **5a**·$CH_2Cl_2$ |
|---|---|---|---|---|---|---|
| Empirical formula | $C_{15}H_{22}BCl_2N_6OW$ | $C_{21}H_{27}BClN_6O_2W$ | $C_{22}H_{29}BClN_6O_3W$ | $C_{47}H_{74}B_2Cl_2N_{12}O_4W_2$ | $C_{50}H_{72}B_2Cl_2N_{14}O_6W_2$ | $C_{28}H_{33}BCl_3N_8O_3W$ |
| Formula weight | 567.95 | 625.60 | 655.62 | 1331.40 | 1425.44 | 830.64 |
| System, space group | Monoclinic, $P2(1)/m$ | Triclinic, $P\bar{1}$ | Triclinic, $P\bar{1}$ | Monoclinic, $C2/c$ | Triclinic, $P\bar{1}$ | Triclinic, $P\bar{1}$ |
| $a$/Å | 8.008(2) | 10.429(4) | 10.872(2) | 11.819(3) | 9.3744(16) | 12.275(4) |
| $b$/Å | 13.970(4) | 11.283(4) | 10.929(5) | 20.631(5) | 10.610(2) | 17.034(7) |
| $c$/Å | 8.963(2) | 11.437(5) | 12.296(4) | 25.873(10) | 14.654(4) | 17.117(5) |
| $\alpha$/° | 90 | 86.39(3) | 68.91(3) | 90 | 97.81(2) | 78.73(2) |
| $\beta$/° | 100.19(2) | 76.986(19) | 82.24(2) | 99.77(2) | 95.395(17) | 75.15(2) |
| $\gamma$/° | 90 | 66.99(2) | 65.41(3) | 90 | 97.33(2) | 70.36(2) |
| $V$/Å$^3$ | 986.9(4) | 1206.5(8) | 1239.4(7) | 6218(3) | 1423.0(6) | 3234.5(18) |
| $Z$ | 2 | 2 | 2 | 4 | 1 | 4 |
| Calc. density/Mg m$^{-3}$ | 1.911 | 1.722 | 1.757 | 1.422 | 1.663 | 1.706 |
| Data/restraints/ parameters | 2358/0/135 | 3355/0/297 | 5633/0/ 335 | 7162/0/303 | 6450/0/359 | 14664/15/806 |
| $\mu$/mm$^{-1}$ | 6.140 | 4.928 | 4.804 | 3.829 | 4.192 | 3.863 |
| $R1$, $wR2$ $[I > 2\sigma(I)]$[b] | 0.0555, 0.1250 | 0.0488, 0.1316 | 0.0320, 0.0792 | 0.0596, 0.1454 | 0.0514, 0.1361 | 0.0652, 0.1632 |

[a] Data in common: $\lambda = 0.71073$ Å; Bruker SMART-CCD diffractometer; $T = 173(2)$ K. [b] The value of $R1$ is based on selected data with $I > 2\sigma(I)$; the value of $wR2$ is based on all data.

**[{W(O)(Tp*)Cl}$_2$(μ-OC$_6$H$_4$C$_6$H$_4$O)] (4).** A mixture of 4,4′-biphenol (0.037 g, 0.20 mmol) and sodium hydride (60% w/w dispersion in mineral oil, 0.016 g, 0.40 mmol) in dry pyridine (20 cm$^3$) was heated to reflux for 30 min to give a pale yellow solution. After cooling to room temperature, $[W(O)(Tp^*)Cl_2]$ (0.250 g, 0.44 mmol) was added, and the mixture was again heated to reflux for 4 days, during which time the solution darkened and became red in colour. The solvent was removed to leave a red–brown solid, which was purified by column chromatography on flash silica with $CH_2Cl_2$. The first, purple band corresponds to a mixture of the starting material (blue) and the desired dinuclear product (red). This was separated from the later-running decomposition products and further purified by chromatography on flash silica with $CH_2Cl_2$–hexane (7 : 3); this allowed the blue contaminant to be separated from the red product **4**. Yield: 0.0563 g, 23%. IR (KBr disc): $\nu$(B–H) 2539, $\nu$(Pz ring) 1542 and $\nu$(W=O) 956 cm$^{-1}$. Anal. calc. for $C_{42}H_{52}N_{12}W_2B_2Cl_2O_4$: C, 40.4; H, 4.2; N, 13.5. Found: C, 39.8; H, 4.4; N, 13.1%. FABMS: $m/z$ 1247 (100%, $M^+$).

**[{W(O)(Tp*)Cl}$_2$(μ-OC$_6$H$_4$N$_2$C$_6$H$_4$O)] (5) and [W(O)(Tp*)-Cl(OC$_6$H$_4$NNC$_6$H$_4$OH)] (5a).** A mixture of 4,4′-azophenol (0.0428 g, 0.20 mmol) and sodium hydride (60% w/w dispersion in mineral oil, 0.016 g, 0.40 mmol) in dry pyridine (20 cm$^3$) was heated to reflux for 30 min to give a dark orange solution. After cooling to room temperature, $[W(O)(Tp^*)Cl_2]$ (0.250 g, 0.44 mmol) was added and the mixture was then heated to reflux for 5 hours, by which time the solution was dark brown in colour. The solvent was removed to leave a brown solid which was purified by column chromatography on flash silica with $CH_2Cl_2$–hexane (1 : 9), giving first a blue band (starting material), then two brown fractions, both of which required further purification.

Further chromatography of the first fraction on flash silica with $CH_2Cl_2$–hexane (3 : 2) produced a brown band of the desired dinuclear complex **5**. Yield: 0.0733 g, 29%. IR (solid): $\nu$(B–H) 2546, $\nu$(Pz ring) 1541 and $\nu$(W=O) 956 cm$^{-1}$. Anal. calc. for $C_{42}H_{52}N_{14}W_2B_2Cl_2O_4$: C, 39.5; H, 4.1; N, 15.4. Found: C, 38.8; H, 4.3; N, 15.0%. FABMS: $m/z$ 1299 (5%, $\{M + Na\}^+$); 1276 (100%, $M^+$).

Further chromatography of the second fraction on flash silica with $CH_2Cl_2$–thf (199 : 1) produced four fractions of which the last to elute (the major constituent) was the mononuclear complex **5a**. Yield: 0.0356 g, 24%. IR (solid): $\nu$(B–H) 2555, $\nu$(Pz ring) 1543 and $\nu$(W=O) 953 cm$^{-1}$. Anal. calc. for $C_{27}H_{31}N_8WBClO_3$: C, 43.5; H, 4.2; N, 15.0. Found: C, 43.8; H, 4.1; N, 14.0%. FABMS: $m/z$ 768 (10%, $\{M + Na\}^+$), 745 (100%, $M^+$).

## X-Ray crystallography

Crystals of the complexes were grown from either $CH_2Cl_2$–hexanes or $CH_2Cl_2$–diethyl ether mixtures by the vapour diffusion technique. In each case a suitable crystal was coated with hydrocarbon oil and attached to the tip of a glass fibre, which was then transferred to a Bruker-AXS SMART diffractometer under a stream of cold $N_2$ at 173 K. Details of the crystal parameters, data collection and refinement for each of the structures are collected in Table 4. After data collection, in each case an empirical absorption correction (SADABS) was applied,[17] and the structures were then solved by conventional direct methods and refined on all $F^2$ data using the SHELX suite of programs.[18] In all cases, non-hydrogen atoms were refined with anisotropic thermal parameters; hydrogen atoms were included in calculated positions and refined with isotropic thermal parameters which were *ca.* 1.2× (aromatic CH) or 1.5× (Me) the equivalent isotropic thermal parameters of their parent carbon atoms. The presence of O/Cl disorder in many cases is discussed in the main text; this could generally be resolved but the resulting W=O and W–Cl distances should be treated with due caution. Complex **3**·$(C_6H_{14})(C_5H_{12})$ lies astride a twofold rotation axis such that only half of the complex molecule is in the asymmetric unit. Disordered solvent molecules were approximated as one hexane and one pentane molecule, lying astride the twofold axis in each case; the geometries of these are irregular and the thermal parameters rather large. Complex **5**·$(Et_2O)_2$ lies across an inversion centre, with half of the complex molecule and one ether molecule in the asymmetric unit. In **5a**·$CH_2Cl_2$ there are two independent complex molecules in the asymmetric unit, of which one is well-behaved, but the other shows disorder about the N=N bond of the azo-phenolate ligand. It was not possible to resolve the two components of the disorder completely; geometric restraints were required to keep the geometry of the N=N bond reasonable.

In all cases the maximum residual electron-density peaks were very close to the tungsten centre, indicating that they arise from absorption effects. Metal–ligand bond distances are collected in Table 1.

CCDC reference numbers 192528–192533.

See http://www.rsc.org/suppdata/dt/b2/b208397c/ for crystallographic data in CIF or other electronic format.

## Acknowledgements

We thank the EPSRC for financial support, and Dr Michael Malaun for assistance with the synthesis of the starting material [W(Tp*)(O)$Cl_2$].

## References and notes

1 Reviews: (*a*) M. D. Ward, *Chem. Soc. Rev.*, 1995, 121; (*b*) F. Paul and C. Lapinte, *Coord. Chem. Rev.*, 1998, **180**, 431; (*c*) W. Kaim, A. Klein and M. Glockle, *Acc. Chem. Res.*, 2000, **33**, 755; (*d*) D. E. Richardson and H. Taube, *Coord. Chem. Rev.*, 1984, **60**, 107; (*e*) K. Kalyanasundaram, *Inorg. Chim. Acta*, 1994, **226**, 213; (*f*) C. Creutz, *Prog. Inorg. Chem.*, 1983, **30**, 1; (*g*) K. D. Demandis, C. M. Hartshorn and T. J. Meyer, *Chem. Rev.*, 2001, **101**, 2655.

2 Recent examples: (*a*) R. H. Laye, S. M. Couchman and M. D. Ward, *Inorg. Chem.*, 2001, **40**, 4089; (*b*) B. J. MacLean and P. G. Pickup, *J. Phys. Chem. B*, 2002, **106**, 4658; (*c*) B. Sarkar, R. H. Laye, B. Mondal, S. Chakraborty, R. L. Paul, J. C. Jeffery, V. Puranik, M. D. Ward and G. K. Lahiri, *J. Chem. Soc., Dalton Trans.*, 2002, 2097; (*d*) D. M. Dattelbaum, C. M. Hartshorn and T. J. Meyer, *J. Am. Chem. Soc.*, 2002, **124**, 4938; (*e*) P. V. Bernhardt, B. P. Macpherson and M. Martinez, *J. Chem. Soc., Dalton Trans.*, 2002, 1435; (*f*) S. Ghosh, K. K. Nanda, A. W. Addison and R. J. Butcher, *Inorg. Chem.*, 2002, **41**, 2243; (*g*) Y. Portilla, I. Chavez, V. Arancibia, B. Loeb, J. M. Manriquez, A. Roig and E. Molins, *Inorg. Chem.*, 2002, **41**, 1831; (*h*) S. Chakraborty, R. H. Laye, V. G. Puranik, M. D. Ward and G. K. Lahiri, *J. Chem. Soc., Dalton Trans.*, 2002, 1172; (*i*) D. P. Arnold, R. D. Hartnell, G. A. Heath, L. Newby and R. D. Webster, *Chem. Commun.*, 2002, 754; (*j*) K. C. Gordon, A. K. Burrell, T. J. Simpson, S. E. Page, G. Kelso, M. I. J. Polson and A. Flood, *Eur. J. Inorg. Chem.*, 2002, 554.

3 (*a*) M. D. Ward and J. A. McCleverty, *J. Chem. Soc., Dalton Trans.*, 2002, 275; (*b*) J. A. McCleverty and M. D. Ward, *Acc. Chem. Res.*, 1998, **31**, 842.

4 (*a*) S. R. Bayly, E. R. Humphrey, H. de Chair, C. G. Paredes, Z. R. Bell, J. C. Jeffery, J. A. McCleverty, M. D. Ward, F. Totti, D. Gatteschi, S. Courric and C. G. Screttas, *J. Chem. Soc., Dalton Trans.*, 2001, 1401; (*b*) N. C. Harden, E. R. Humphrey, J. C. Jeffery, S.-M. Lee, M. Marcaccio, J. A. McCleverty, L. H. Rees and M. D. Ward, *J. Chem. Soc., Dalton Trans.*, 1999, 2417; (*c*) V. A. Ung, D. A. Bardwell, J. C. Jeffery, J. P. Maher, J. A. McCleverty, M. D. Ward and A. Williamson, *Inorg. Chem.*, 1996, **35**, 5290.

5 (*a*) A. McDonagh, S. R. Bayly, D. J. Riley, M. D. Ward, J. A. McCleverty, M. A. Cowin, C. N. Morgan, R. Varrazza, R. V. Penty and I. H. White, *Chem. Mater.*, 2000, **12**, 2523; (*b*) S.-M. Lee, M. Marcaccio, J. A. McCleverty and M. D. Ward, *Chem. Mater.*, 1998, **10**, 3272.

6 (*a*) S. Bayly, J. A. McCleverty, M. D. Ward, D. Gatteschi and F. Totti, *Inorg. Chem.*, 2000, **39**, 1288; (*b*) V. A. Ung, S. M. Couchman, J. C. Jeffery, J. A. McCleverty, M. D. Ward, F. Totti and D. Gatteschi, *Inorg. Chem.*, 1999, **38**, 365; (*c*) V. A. Ung, A. M. W. Cargill Thompson, D. A. Bardwell, D. Gatteschi, J. C. Jeffery, J. A. McCleverty, F. Totti and M. D. Ward, *Inorg. Chem.*, 1997, **36**, 3447.

7 (*a*) A. A. Eagle, G. N. George, E. R. T. Tiekink and C. G. Young, *Inorg. Chem.*, 1997, **36**, 472; (*b*) A. A. Eagle, R. W. Gable and C. G. Young, *Aust. J. Chem.*, 1999, **52**, 827; (*c*) A. A. Eagle, G. N. George, E. R. T. Tiekink and C. G. Young, *J. Inorg. Biochem.*, 1999, **76**, 39; (*d*) A. A. Eagle, E. R. T. Tiekink and C. G. Young, *Inorg. Chem.*, 1997, **36**, 6315; (*e*) A. A. Eagle, S. M. Harben, E. R. T. Tiekink and C. G. Young, *J. Am. Chem. Soc.*, 1994, **116**, 9749.

8 (*a*) C. D. Garner and L. J. Stewart, *Met. Ions Biol. Syst.*, 2002, **39**, 699; (*b*) C. G. Young and A. G. Wedd, *Chem. Commun.*, 1997, 1251; (*c*) J. McMaster and J. H. Enemark, *Curr. Opin. Chem. Biol.*, 1998, **2**, 201.

9 G. Ferguson, B. Kaitner, F. J. Lalor and G. Roberts, *J. Chem. Res. (S)*, 1982, **1**, 6.

10 A. Bencini, D. Gatteschi, J. A. McCleverty, D. N. Sanz, F. Totti and M. D. Ward, *J. Phys. Chem. A*, 1998, **102**, 10545.

11 F. E. Mabbs and D. Collison, *Electron Paramagnetic Resonance of d Transition Metal Compounds*, Elsevier, Amsterdam, 1992.

12 (*a*) F. M. Horning and W. Kaim, *J. Chem. Soc., Faraday Trans.*, 1994, **90**, 2909; (*b*) C. A. Rice, P. M. H. Kroneck and J. T. Spence, *Inorg. Chem.*, 1981, **20**, 1996; (*c*) F. M. Horning, O. Heilmann, W. Kaim, S. Zalis and J. Fiedler, *Inorg. Chem.*, 2000, **39**, 4052; (*d*) E. S. Davies, G. M. Aston, R. L. Beddoes, D. Collison, A. Dinsmore, A. Docrat, J. A. Joule, C. R. Wilson and C. D. Garner, *J. Chem. Soc., Dalton Trans.*, 1998, 3647; (*e*) B. A. Goodman and J. B. Raynor, *Adv. Inorg. Chem. Radiochem.*, 1970, **13**, 135.

13 If $[\mathbf{3}]^+$ were delocalised on the EPR timescale in fluid solution, we would see a superposition of a singlet [73% of total intensity, arising from the W nuclear spin combination $I = (0, 0)$]; a doublet [25%, arising from the $I = (0, 1/2)$ combination] and a triplet [2%, arising from the $I = (1/2, 1/2)$ nuclear spin combination]; the separation between components in the doublet and triplet would be half the value observed in a mononuclear complex (see ref. 3*b*). Given the broadness of the signals, the practical effect would be that the intensity of the two visible hyperfine components (from a doublet in a localised complex) would be greatly reduced in intensity, replaced by the outer components of a very low-intensity triplet in the same position. The fact that the intensity of these satellites is the same for $[\mathbf{3}]^+$ as it is for **1** means that they arise from a doublet (with 14.3% relative intensity) and not a triplet (with 2% relative intensity); this confirms valence localisation on the EPR timescale in solution.

14 S.-M. Lee, R. Kowallick, M. Marcaccio, J. A. McCleverty and M. D. Ward, *J. Chem. Soc., Dalton Trans.*, 1998, 3443.

15 (*a*) C. J. O'Connor, *Prog. Inorg. Chem.*, 1982, **29**, 203; (*b*) R. L. Carlin, *Magnetochemistry*, Springer Verlag, New York, 1986.

16 C. Persson and C. Andersson, *Inorg. Chim. Acta*, 1993, **203**, 235.

17 G. M. Sheldrick, SADABS, A program for absorption correction with the Siemens SMART area-detector system, University of Göttingen, 1996.

18 G. M. Sheldrick, SHELXS-97 and SHELXL-97 programs for crystal structure solution and refinement, University of Göttingen, 1997.